Title

Improving the distribution of Doxil® in the tumor matrix by depletion of tumor hyaluronan

Permalink

https://escholarship.org/uc/item/98g7s5ck

Authors

Kohli, Aditya G
Kivimäe, Saul
Tiffany, Matthew R
et al.

Publication Date

2014-10-01

DOI

10.1016/j.jconrel.2014.05.019

Peer reviewed

Improving the distribution of Doxil® in the tumor matrix by depletion of tumor hyaluronan

Aditya G. Kohli[1,2], **Saul Kivimäe**[2], **Matthew R. Tiffany**[2,3], and **Francis C. Szoka**[1,2,3]

[1]The UC-Berkeley-UCSF Graduate Program in Bioengineering, University of California Berkeley, Berkeley, CA 94720

[2]Department of Bioengineering, Therapeutic Sciences and Pharmaceutical Chemistry, University of California San Francisco, San Francisco, CA 94143

[3]Pharmaceutical Sciences and Pharmacogenomics Graduate Program, Department of Bioengineering and Therapeutic Sciences, University of California, San Francisco, CA 94143

Abstract

Liposomes improve the pharmacokinetics and safety of rapidly cleared drugs, but have not yet improved the clinical efficacy compared to the non-encapsulated drug. This inability to improve efficacy may be partially due to the non-uniform distribution of liposomes in solid tumors. The tumor extra-cellular matrix is a barrier to distribution and includes the high molecular weight glycosaminoglycan, hyaluronan (HA). Strategies to remove HA or block its synthesis may improve drug delivery into solid tumors. Orally administered methylumbelliferone (MU) is an inhibitor of HA synthesis, but it is limited by low potency and limited solubility. In this study, we encapsulate a water-soluble phosphorylated prodrug of MU (MU-P) in a liposome (L-MU-P). We demonstrate that L-MU-P is a more potent inhibitor of HA synthesis than oral MU in the 4T1 murine mammary carcinoma model using both a quantitative ELISA and histochemistry. We show that HA depletion improves the tumor distribution of liposomes computed using Mander's colocalization analysis of liposomes with the tumor vasculature. Hyaluronan depletion also increases the fraction of the tumor area positive for liposomes. This improved distribution extends the overall survival of mice treated with Doxil®.

Keywords

Liposomes; tumor penetration; extra-cellular matrix; breast cancer

Corresponding Author: Francis C. Szoka, szoka@cgl.ucsf.edu, School of Pharmacy, University of California, 513 Parnassus Ave., Box 0912, San Francisco, CA, 94143, USA, 415-476-3895, Francis Szoka, szoka@cgl.ucsf.edu.

Conflict of Interest

F.C.S. declares a conflict of interest due to his involvement in a liposome company. The other authors declare no conflict of interest.

Contributions

A.G.K. and F.C.S conceived and designed the experiments. A.G.K. performed experiments. S.K. conducted animal experiments. M.R.T. helped with qPCR studies. A.G.K analyzed the data. A.G.K. and F.C.S. wrote the paper.

Publisher's Disclaimer: This is a PDF file of an unedited manuscript that has been accepted for publication. As a service to our customers we are providing this early version of the manuscript. The manuscript will undergo copyediting, typesetting, and review of the resulting proof before it is published in its final citable form. Please note that during the production process errors may be discovered which could affect the content, and all legal disclaimers that apply to the journal pertain.

Introduction

Nanoparticle therapeutics, especially liposomes, have been investigated as anti-cancer drug carriers for four decades with a number of clinical and commercial successes [1]. Encapsulating a drug in a liposome extends its circulation time and improves its biodistribution. Successful delivery of liposomes into a tumor depends on: 1) prolonged circulation in the bloodstream, 2) extravasation from the tumor vasculature, and 3) distribution into the tumor parenchyma. The large diameter of nanoparticles allows for their selective accumulation at the tumor site by the enhanced permeability and retention (EPR) effect [2,3]. However, the diameter of liposomes is a double-edged sword: while a boon for drug loading, pharmacokinetics, and biodistribution, it limits distribution in the tumor [2–4]. As a result, despite improved pharmacokinetics, liposome therapies have offered limited improvements in efficacy over the un-encapsulated drug [3].

Liposome distribution away from the vasculature is limited by both the steric barrier of the tumor extracellular matrix (ECM) and the elevated tumor interstitial fluid pressure (IFP) [5]. A myriad of molecular approaches have been used to improve the tumor distribution of macromolecular therapeutics including: tumor penetrating peptides [6–8], hyperthermia [9,10], degradable nanoparticles [11], enzymes and small molecules that modify the tumor ECM [12–16], vascular priming [17], and vascular normalization [18,19]. The effectiveness of these approaches depends on the pharmacology of the drug and the biology of the tumor. While certain tumors may exhibit a pronounced EPR effect, others do not [20]; further, while a subset of tumors have an ECM rich in collagen, others have an ECM rich in hyaluronan. As such, each tumor type presents a different physical barrier to delivery, and this heterogeneity calls for a number of potential approaches to improve tumor distribution.

The tumor ECM is composed of a network of collagen and hyaluronic acid (HA) that interact with other hydrated proteoglycans. The matrix contributes to the high IFP by entrapping water and prevents penetration of liposomes into the tumor core [21]. HA is an intractable barrier to liposome drug delivery and hence a potential therapeutic target. A high molecular weight glycosaminoglycan, HA is enriched in human breast, colorectal, gastric, glioma, lung and ovarian tumors [22–26]. Nearly 90% of human pancreatic adenocarcinomas are characterized by abundant accumulation of HA [27,28]. HA is involved in tumor progression; high levels correlate with the motility, invasiveness, and metastatic potential of tumor cells [29,30]. HA directs cell motility by interacting with cell receptors CD44 and RHAMM and can shield tumor cells from host immune cells [31]. For the above reasons, strategies to remove HA or block its synthesis could improve drug delivery into solid tumors.

Given its abundance across tumor types and role in metastasis, HA has been the target of various therapeutic interventions [32–34]. Systemic administration of PEGPH20 (Halozyme Therapeutics), a PEGylated human hyaluronidase, transiently depleted HA, decreased tumor IFP, and enhanced drug activity in prostate and pancreatic tumor models [32,35]. Further, PEGPH20 improved the uptake and distribution of liposomal doxorubicin in osteosarcoma

xenograft models [36]. PEGPH20 is currently being investigated in combination with gemcitabine in clinical trials for pancreatic cancer (NCT01453153).

A small molecule, 4-methylumbelliferone (MU), has also been used to deplete HA and reduce metastasis in solid tumors [33,37–40] and has been extensively evaluated *in vitro* [33,41–43]. MU is a safe, well characterized, and clinically approved cholorectic and antiplasmodic agent [44–48]. MU inhibits HA synthesis by down-regulating hyaluronan synthase 2 and 3 (HAS2, HAS3) and by depleting the cellular pool of UDP-glucuronic acid, one of the building blocks of HA (Figure 1A) [33,49]. However, MU is limited by its low potency (daily oral doses of 450mg/kg) [33] and low water solubility.

In this study, we circumvent these limitations of MU by encapsulating a water-soluble phosphorylated prodrug of MU (MU-P) in a liposome (L-MU-P). Phosphorylated prodrugs have previously been encapsulated in liposomes (reviewed in [50]). We demonstrate that L-MU-P is a more potent inhibitor of HA synthesis than oral MU in the 4T1 murine mammary carcinoma model. We further demonstrate that, under certain conditions, HA depletion improves the tumor distribution of liposomes, which results in enhanced anti-tumor efficacy.

Results

MU-P depletes HA in culture media

MU-P is rapidly dephosphorylated over the course of minutes to form MU in serum (Figure 1B) and in a number of tissue homogenates [51]. This conversion is slower in heat-inactivated serum, indicating a loss in endemic serum phosphatases (data not shown). HA-rich 4T1 murine mammary carcinoma cells [32] and HA-poor C26 murine colon carcinoma cells were used as model systems to test MU-P mediated HA depletion. MU and MU-P reduced HA levels in culture media of 4T1 cells in a dose-dependent manner (Figure 1C). Blocking MU-P dephosphorylation by including a phosphatase inhibitor in the media decreased the activity of HA synthesis inhibition of MU-P. Conversely, MU and MU-P had little effect on the low levels of HA found in C26 culture media (Supplementary Figure 1A). Measurements of HA levels were normalized to cell number in order to account for cell cytotoxicity of MU and MU-P at high concentration.

Characterization of liposomal MU-P

MU-P was passively encapsulated in a range of liposome formulations and its rate of release from each formulation was quantified using a simple *in vitro* assay [51]. Two MU-P encapsulating formulations, *HSPC* and *POPC*, were selected for further study (Figure 2A). These liposome formulations had similar diameter, zeta-potential, and encapsulation efficiency (Figure 2A,B). However, in serum the formulations demonstrated different leakage rates of MU-P. While MU-P is stably encapsulated in the *HSPC* formulation, it slowly leaks from the *POPC* formulation at 37 °C in 30% fetal bovine serum (Figure 2C). This difference in leakage rates is mirrored *in vivo*. While both formulations dramatically extended the circulation time of MU-P compared to the free drug, MU-P leaked faster from *POPC* liposomes than from *HSPC* liposomes in circulation (Figure 2D). We hypothesized

that the rapid yet steady release profile of MU-P from *POPC* liposomes would lead to a sustained reduction of HA at the tumor site.

Liposomal MU-P depletes HA in 4T1 tumors

To investigate the activity of L-MU-P as an inhibitor of HA synthesis, *POPC* MU-P was evaluated in the 4T1 tumor model. The 4T1 model is a good surrogate for human breast tumors, since this model overexpresses *HAS2,* readily metastasizes, and is rich in HA as are more than 50% of human breast tumors [38,52]. L-MU-P was administered intravenously while MU was given by oral gavage (450 mg/kg/day) (Figure 3A). At all dose levels, L-MU-P reduced tumor HA to a greater extent than oral MU as determined by an HA ELISA assay (Figure 3B). This result was corroborated by histochemistry, as Alcian Blue staining of HA is reduced in a dose dependent fashion (Figure 3C). In contrast, L-MU-P had little effect on HA levels in HA-low C26 tumors (Supplementary Figure 1B). L-MU-P had no effect on 4T1 tumor growth or metastatic progression (Figure 7; Supplementary Figure 2A,B).

In order to understand the exposure of the tumor to MU-P, we measured the "cellular availability" of L-MU-P liposomes in 4T1 tumors. This term describes the fraction of drug released from the liposome and available for therapeutic activity [51]. The presence of both MU and MU-P in the tumor 48 hours after administration indicates the persistence of intact liposomes, and the presence of MU supports the hypothesis of sustained MU-P release from liposomes to inhibit HA synthesis (Figure 3D).

We also measured the effect of HA depletion on Doxil® accumulation in the tumor. Interestingly, HA depletion by L-MU-P did not lead to an increase in Doxil® accumulation in the tumor (Figure 3E), indicating that HA depletion by L-MU-P does not enhance the EPR effect and improve tumor uptake of nanoparticle therapeutics.

Liposomes interact with macrophages in the tumor microenvironment

We further analyzed the mechanism of L-MU-P action in the tumor. Tumor HA is synthesized by tumor cells, rather than stromal cells [53]. MU-P interacts with tumor cells after being released from the liposome. MU-P may be released from liposomes in tumor cells, and may also be released after uptake into phagocytic cells in the tumor. Liposomes colocalized with macrophages in the 4T1 tumor (Figure 4A). After HA depletion with L-MU-P, the extent of liposome colocalization with macrophages and the number of macrophages in the tumor were unaltered (Figure 4B,C). While the colocalization analysis does not conclusively show that the liposomes are internalized in the macrophages, it does suggest that the liposomes and macrophages are in close proximity. Further, liposomes colocalized with both tumor cells and tumor macrophages, but only a small fraction of macrophages colocalized with liposomes. The uniform presence of macrophages throughout the tumor (Figure 4D) may thus catalyze MU-P release.

MU-P *in vivo* activity is not due to down-regulation of *HAS2*

While MU may inhibit HA synthesis by depleting cellular glucuronic acid, it may also do so by reducing levels of *HAS2* [33,49]. *HAS2* is an established oncogene and is over-expressed

in a number of murine and human mammary tumors [38]. We found that *HAS2* is the most prevalent HA synthase in 4T1 tumors both *in vitro* and *in vivo* (Figure 5A,C). Further, *in vitro*, MU selectively reduced *HAS2* expression *in vitro* while having little effect on *CD44* and *HAS3* expression levels (Figure 5B). In contrast, *in vivo*, L-MU-P had little effect on *HAS2* levels. This result may be due to an insufficient amount of MU in the tumor to influence gene expression (Figure 5D).

HA depletion improves liposome distribution in 4T1 tumors

After confirming that L-MU-P reduced HA levels in 4T1 tumors, we examined if HA depletion altered the distribution of liposomes. To that end, we injected DiD labeled empty liposomes intravenously in mice with 4T1 tumors, removed the tumors 24 hours later, prepared sections of the tumors, and quantified the liposome distribution by microscopy (Figure 6; Supplementary Figure 3). The tumor distribution of labeled liposomes was quantified across the entire tumor using two metrics: 1) the degree of colocalization between the liposome DiD signal and endothelial cell marker CD31 and 2) total tumor area positive for liposome signal (Figure 6D,E). Both metrics are described in further detail in Materials and Methods, and images of entire tumor sections are presented in the Supplementary Information (Supplementary Figure 3).

Liposomes enter the tumor by escaping the porous vasculature via the EPR effect and then permeate into the tumor parenchyma by diffusion [54]. This distribution away from endothelial cells can be quantified by computing the colocalization of the liposome signal (DiD) and vasculature signal (CD31) across the entire tumor. If the liposomes do not leave the vasculature, the two signals will be perfectly colocalized and the fraction of non-colocalized liposomes will be low. In contrast, if the liposomes distribute away from the vasculature, the fraction of non-colocalized liposomes will be high. An alternate approach to computing liposome distribution is to examine the entire tumor area for liposome signal. Tumors with a greater fraction of area positive for liposomes may have a greater exposure to the liposome encapsulated drug as it is released in the tumor.

In 4T1 tumors, liposomes are confined to the area immediately surrounding the vasculature (Figure 6B, Supplementary Figure 3A,B) and exhibit a low fraction of non-colocalized liposomes (Figure 6D). After HA depletion, DiD labeled liposomes distributed away from the vasculature (Figure 6C, Supplementary Figure 3C,D), and this distribution is reflected by a higher fraction of non-colocalized liposomes (Figure 6D). Similarly, the fraction of total tumor area positive for liposomes significantly increased after HA depletion (Figure 6E). These results demonstrate that HA depletion by L-MU-P increases the distribution of liposomes in HA-rich tumors.

Improved liposome distribution improves efficacy of Doxil®

Based on this improved tumor distribution, we hypothesized that HA depletion would increase the efficacy of Doxil®, and we next investigated if L-MU-P given with Doxil® or with non-encapsulated doxorubicin altered the anti-tumor effect of the drug. HA depletion using a four-dose regime of L-MU-P was followed by a single dose of Doxil® (Figure 7A). The combination of L-MU-P and Doxil® had greater anti-tumor efficacy than Doxil®

monotherapy. The combination therapy slowed tumor growth and improved overall survival (Figure 7B,C), but did not improve Doxil® uptake into 4T1 tumors (Figure 3E). The efficacy of higher doses of Doxil® (10 mg/kg and 20 mg/kg) were not improved by HA depletion (Supplementary Figure 4), suggesting that there is an optimal dose window of Doxil® where efficacy is improved by increased penetration. In contrast to Doxil®, L-MU-P did not improve the efficacy of free doxorubicin (Supplementary Figure 2C,D). This result is not surprising, as the distribution of small molecule drugs is less hindered than that of nanoparticles.

Discussion

HA is recognized as an important target in oncology because of its role in tumor progression and abundance across a range of solid tumors [55]. Therapies that target HA may be widely applicable and may slow tumor progression as a monotherapy or improve the effect of another therapeutic in a combination therapy [32,35]. In this study, we build on previous work that validates MU as an inhibitor of HA synthesis to demonstrate that 1) encapsulation of a prodrug of MU (MU-P) in a liposome (L-MU-P) effectively depletes tumor HA, 2) HA depletion improves liposome distribution, and 3) improved distribution improves Doxil® efficacy and extends overall survival.

In comparison to other methods to deplete HA in tumors, such as oral MU or PEGPH20, our studies implicate increased tumor distribution of Doxil® as the mechanism for improved efficacy rather than improved Doxil® uptake, MU cytotoxicity, or altered HA synthase gene expression. In contrast to PEGPHG20 treatment, treatment with L-MU-P does not alter the EPR effect and enhance tumor uptake of nanoparticles [56]. PEGPH20 depletes HA over the course of hours, but L-MU-P depletes HA over the course of days. This difference in kinetics may allow the tumor vasculature to adapt to changes in the microenvironment, which may prevent improved uptake of liposomes into the tumor. For example, PEGPH20 may transiently reduce the IFP gradient across the wall of tumor blood vessels and increase extravasation of therapeutics into the tumor [55]. Further, PEGPH20 slows tumor growth as a monotherapy [32], although this may be partially driven by the tumor collapsing on itself without the presence of the HA matrix.

At the doses administered in this study, L-MU-P does not have an anti-tumor effect as a monotherapy (Figure 6) and may not catastrophically alter the tumor microenvironment in the same way as PEGPH20. L-MU-P has no effect on expression of *HAS2* and *HAS3* in the tumor although MU has previously been reported to slow tumor progression and affect *HAS2* expression levels. However, these *in vitro* studies used high doses of MU that may not be achievable in the tumor [33]. As such, increasing the dose of L-MU-P may have the additional benefit of altering gene expression.

MU is a clinically approved agent that is safe in humans at high doses [44–48]. HA is abundant in a number of tissues throughout the body including the skin and joints and is intimately involved in wound healing and inflammation [57]. For this reason, careful attention should be paid to the potential off-target toxicities of agents that target tumor HA.

At the doses administered in this study, L-MU-P demonstrated no toxicity in mice. However, this safety profile may not hold for more potent inhibitors of HA synthesis.

In this study, we demonstrate that L-MU-P is a useful tool for increasing the efficacy of liposome therapeutics (Figure 6). In addition to liposomes, L-MU-P may be used to improve the distribution of other macromolecular therapeutics including antibodies, proteins and cell-based therapies. However, the low potency of MU and its derivatives still limit their clinical use. Future work should be focused on developing more potent and specific inhibitors of *HAS2* and *HAS3* as combination therapies to augment distribution and efficacy of macromolecular therapeutics in HA rich tumors.

Materials and Methods

Lipids

L-α-phosphatidylcholine hydrogenated (HSPC), 1-palmitoyl-2-oleoyl-*sn*-glycero-3-phosphocholine (POPC), 1,2-distearoyl-*sn*-glycero-3-phosphoethanolamine-N-[methoxy(polyethylene glycol)-2000] (DSPE-PEG), and cholesterol were purchased from Avanti Polar Lipids. 1,1-dioctadecyl-3,3,3,3- tetramethylindodicarbocyanine (DiD, excitation 644 nm, emission 664 nm) was obtained from Life Technologies.

Antibodies, dyes and tracer molecules

MU (excitation 360 nm, emission 449 nm), MU-P (excitation 320 nm, emission 385 nm), methylumbelliferyl sulfate (MU-S), methylumbelliferyl glucuronide (MU-G), and 7-hydroxycoumarin were obtained from Sigma. Purified rat anti-mouse CD31 (clone MEC 13.3) was purchased from BD Pharmingen. Purified rat anti-mouse CD68 (clone FA-11) was purchased from AbD Serotec. Secondary FITC-conjugated donkey anti-rat IgG (712–095–153) was purchased from Jackson ImmunoResearch Laboratories. Hoechst 3342 nuclear stain was purchased from Thermo Scientific.

Instrumentation

Solvents were removed under reduced pressure using a rotary evaporator. Fluorescence spectroscopy was measured on a FluoroLog-3 spectrofluorimeter (Horiba Jobin Yvon) equipped with a temperature-controlled stage (LFI-3751) or using a Tecan Infinite 4300 (Tecan Group Ltd). Data acquisition was done through FluorEssence software (Horiba Scientific). High-pressure liquid chromatography (HPLC) was performed on an Agilent 1100 HPLC (Agilent).

MU-P hydrolysis in serum

MU-P or MU-S were dissolved in phosphate buffered saline (2.7mM KCl, 1.5mM KH_2PO_4, 136.9mM NaCl, 8.9mM Na_2HPO_4, pH 7.4; PBS) and incubated with 10–50% human, mouse, chicken, goat, rabbit, porcine, or fetal bovine serum at 37°C. All serum was purchased from Gibco. Prodrug conversion to MU was monitored by measuring MU fluorescence (excitation 360, emission 449) every 5 minutes over 12 hours. Data was fit to a Michaelis-Menten model using GraphPad Prism.

Quantification of HA in cell culture

4T1 murine breast carcinoma cells were seeded in 96 well cell culture plates (Corning Costar) at 5,000 cells per well. Cells were cultured in RPMI 1640 media supplemented with 10% fetal bovine serum. MU was solubilized in dimethyl sulfoxide (DMSO), diluted into RPMI 1640 media supplemented with insulin, transferrin, and sodium selenite (ITS, Sigma)), and added to cells. MU-P was solubilized directly into RPMI-ITS and added to cells. Twenty-four hours after plating, cells were washed 3x with phosphate buffered saline (2.7mM KCl, 1.5mM KH_2PO_4, 136.9mM NaCl, 8.9mM Na_2HPO_4, pH 7.4; PBS). MU and MU-P were added to cells after washing with or without Phosphatase Inhibitor Cocktail 2 (Sigma). Forty-eight hours later, 50 μL of media was removed and frozen. Fifteen μL of alamarBlue (Life Technologies) was added to cell media and incubated for 3 hours. Cell number was quantified by measuring alamarBlue fluorescence at 585 nm after excitation at 570 nm using a Tecan Infinite 4300 (Tecan Group Ltd).

HA levels in culture media were quantified by using the HA DuoSet ELISA assay (R&D Systems). Frozen media samples were thawed and diluted 1:100 in Reagent Diluent (R&D Systems). The ELISA was run according to the manufacturer's specifications. Total HA in culture media was normalized to cell number using the alamarBlue assay and to DMSO control wells.

Liposome preparation

Liposomes that were used in animals were prepared by an ethanol injection method followed by extrusion. Dry lipid powders were weighed out and solubilized in 2 mL of ethanol. After warming to 65 °C, lipids were rapidly injected into a heated 18 mL solution of 300 mM MU-P or Hepes buffered saline (HBS; 10mM Hepes, 140mM NaCl, pH 7.4) for control and DiD labeled liposomes. Two liposome formulations were adiminstered in the HA depletion and survival studies: POPC:Cholesterol:DSPE-PEG (55:40:5) and HSPC:Cholesterol:DSPE-PEG (55:40:5). In the liposome distribution study, POPC:Cholesterol:DSPE-PEG:DiD (55:40:5:0.2) was used. The solution was serially extruded through polycarbonate membranes using a high-pressure lipid extruder (Northern Lipids) heated to 65 °C: 4x through a 200 nm membrane, 4x through a 100 nm membrane, and 2x through an 80 nm membrane. Lipids were then dialyzed against HBS with frequent buffer exchange. Before use, liposomes are sterilized by filtration through a 0.2 μm membrane. MU-P loading was measured by lysing liposomes and fitting MU-P fluorescence to a standard curve. Average liposome diameter and zeta potential measurements were determined using the Zetasizer Nano ZS (Malvern Instruments). Zeta potential was fit using the Smoluchowski model, while Mark Houwink parameters were used to determine diameter. All samples were run in triplicate. Release of MU-P from liposomes was quantified as previously described [51].

Transmission electron microscopy (TEM)

TEM images were obtained at the University of California Berkeley Robert D. Ogg Electron Microscope Laboratory. Ten μL of liposome solutions were added to glow discharged copper grids with 400 mesh and Formvar/carbon coatings from Structure Probe, Inc. (West Chester, PA). Liposomes were allowed to adsorb on grids for 2 min. Grids were washed three times with distilled water. Liposomes were negatively stained with 1% uranyl acetate

and excess stain was removed with by a single wash with distilled water. Grids were imaged using an FEI Tecnai 12 TEM (FEI, Hillsboro, OR).

HA depletion in tumors

All animal experiments were performed in compliance with the NIH guidelines for animal research under a protocol approved by the Committee on Animal Research at the University of California, San Francisco. Female BALB/c mice were injected with 300,000 4T1 cells into the mammary fat pad in a volume of 50 μL RPMI media. Mice were treated with MU or L-MU-P to reduce tumor HA levels. MU was dosed daily by oral gavage at 400 mg/kg 5 days a week. MU was mixed in a 1% carboxymethylcellulose (CMC) solution in a volume of 1 mL per dose. L-MU-P was dosed intravenously at a dose of 18 mg/kg MU-P in a volume of 0.2 mL. L-MU-P was administered in 1–4 doses on days 14, 17, 20, and 24. Forty-eight hours after the final dose, tumors were isolated, homogenized in lysis buffer (0.1% Triton X-100 in PBS), and then rotated in lysis buffer for 48 hours at 4 °C [58]. Homogenates were centrifuged at 6500g for 1 hour and then 13000g for 1 hour and the supernatants were collected. Samples were diluted 1:500 before adding to the ELISA plate. The ELISA was run according to the manufacturer's specifications. Total tumor HA was normalized to the weight of the tumor sample.

Tissue immunofluorescence

Organs were isolated from mice and snap frozen. Organs were embedded in O.C.T. compound (Tissue-Tek) and sectioned into 20 μm sections and stored at −20 °C. Sections were fixed in acetone for 5 minutes at −20 °C and washed 3x with PBS. Sections were blocked with blocking buffer (1% goat serum, 1% BSA, PBS) for 2 hours at room temperature. Anti-CD31 antibody was added to sections at a 1:100 dilution in blocking buffer for 1 hour at room temperature. Anti-CD68 antibody was added to sections at a 1:100 dilution in blocking buffer overnight at 4 °C. After 3 washes in PBS, secondary antibody was added at a 1:400 dilution in blocking buffer for 40 minutes at room temperature. After another 3 washes in PBS, sections were incubated with Hoechst nuclear stain at a 1:1000 dilution in blocking buffer for 20 minutes at room temperature. After 3 washes in PBS, sections were mounted using ProLong Gold anti-fade reagent (Life Technologies). Sections were imaged 24 hours after mounting.

Cell culture immunofluorescence

4T1 cells were plated directly on poly-lysine coated glass slides. Primary macrophages were isolated by plating total bone marrow in Dulbecco's Modified Eagle Medium (DMEM) supplemented with 10% FBS and 20 ng/mL M-CSF1. Primary macrophages were plated on uncoated glass slides. After reaching 80% confluence, cells were fixed with chilled acetone and washed 3x with PBS. Slides were blocked for 1 hour at room temperature and stained with anti-CD68 antibody as outlined above.

Immunohistochemistry

Organs were isolated from mice and immediately placed in 70% ethanol, 5% glacial acetic acid, 4% formalin solution for 48 hours [59]. Organs were embedded in paraffin, cut into 20

μm sections, and hydrated by serial washes through Clear-Rite (Thermo Scientific), 100% ethanol, 50% ethanol, 10% ethanol and deionized water. Hydrated sections were washed three times in deionized water and placed in 3% acetic acid solution for 3 minutes. Slides were incubated in 1% Alcian Blue solution pH 2.5 for 30 minutes at room temperature. Sections were rinsed with tap water for 5 minutes and deionized water for 5 minutes and then incubated with Nuclear Fast Red (Sigma) for 5 minutes. Sections were rinsed for 5 minutes in deionized water and then dehydrated and mounted with Permount (Fisher Scientific). Sections were imaged 24 hours after mounting. Control sections were incubated with hyaluronidase from bovine testes (Sigma H3884) for 1 h at 37 °C before the incubation with acetic acid.

qPCR

mRNA was isolated from cells in culture or tissue samples using Trizol reagent according to the manufacturers protocol (Life Technologies). The SuperScript III First-Strand Synthesis System for RT-PCR was used to convert mRNA to cDNA. Oligo(dT)$_{20}$ primers were used for first strand synthesis of 5 μg total RNA. Primer sets are shown below and were purchased from Integrated DNA Technologies:

Primer	Sequence	Optimal concentration (nM)
HAS1 F	GAGAACAAGACGGAGAAGAGAG	900
HAS1 R	AGGATGAGCAGGGCAAAG	900
HAS2 F	CTATGCTTGACCCTGCCTC	300
HAS2 R	AAAGCCATCCAGTATCTCACG	300
HAS3 F	GAAGCCAGAACAGTATAGCCTG	300
HAS3 R	CAGCCATGAAACTAGAACACAAC	900
CD44 F	CAACACCTCCCACTATGACAC	300
CD44 R	CTGTAGCGAGTACCATCACG	900

Fifty ng of cDNA was combined with both forward and reverse primer at the above concentrations along with FastStart Universal SYBR Green Master (Roche). The reaction was run on a Stratagene Mx3005P RT-PCR machine with the following program: 1 cycle (95 °C for 10 s), 70 cycles (95 °C for 15 s, 60 °C for 60 s), 1 cycle (95 °C for 60 s, 55 °C for 30 s, 95 °C for 30 s). Primer dimer sets were removed by analysis of the dissociation curves. C_T values for each gene were determined from amplification curves and delta C_T values were computed against a B-actin control. Murine B-actin primers were purchased from MCLAB

Liposome distribution studies

Liposome distribution in tumors was measured by tracking liposomes labeled with DiD in 4T1 tumors. Mice were dosed with 4 doses of 18 mg/kg equivalents of 0.2 mL of L-MU-P or PBS by intravenous tail vein injection on days 9, 13, 16, and 19 after tumoring. On day 20, mice were dosed with empty liposomes labeled with DiD. On day 21, mice were sacrificed and tumors were isolated and snap frozen for immunofluorescence.

Tumor imaging and analysis

Tumor sections were imaged on a Nikon Ti-E microscope and processed using NIS Elements 4.20 (Nikon) and Fiji [60]. Three-channel images were captured on the microscope: nuclear stain Hoechst3342, CD31 stain FITC or CD68 stain FITC; and lipid membrane dye DiD. Imaging and exposure settings remained consistent through all experiments. Tumors were imaged at 20x and large composite images were stitched together using the NIS Elements software. When collecting large images, the microscope was refocused on every second image and exposure times and microscope settings remained constant across all samples. Each channel was saved in a separate TIFF file and loaded in Fiji. Background was subtracted from images using a Rolling Ball background subtraction with a radius of 50. Then an absolute background subtraction of a pixel value of 1500 was applied. To quantify the % positive area for DiD or CD68, the tumor region of interest (ROI) was selected and the % area was measured using the "Measure %Area" function. To further quantify the extent of colocalization between CD31 blood vessels or CD68 macrophages and DiD liposomes, Mander's colocalization analysis was performed across the entire tumor and the extent of colocalization between the DiD and CD31 signal is reported [61].

Survival studies

Mice were dosed with 4 doses of 18 mg/kg equivalents of L-MU-P or PBS (0.2 mL) by intravenous tail vein injection on days 4, 8, 11, and 14 after tumoring. On day 15, mice were given a single intravenous dose of Doxil® at 6 mg/kg or 10 mg/kg or PBS. Mice were then monitored daily until removal from the study by IACUC guidelines. Tumor dimensions were measured with digital calipers and tumor volume was determined by taking two perpendicular measurements [62]. Kaplan Meier plots were generated using GraphPad Prism.

HPLC tissue analysis of MU-P and doxorubicin

Tissues were analyzed for MU-P and metabolites as previously reported [51]. Briefly, tumors were homogenized in the presence of Phosphatase Inhibitor Cocktail 2 (Sigma), MU-P and metabolites were extracted into the homogenization solution (50% Methanol, 0.1% TFA, 1:100 dilution of, 1 μg/mL 7-hydroxycoumarin as an internal standard). After centrifugation, samples were injected on a C_8 column (ZORBAX Eclipse XDB-C8 5-Micron). To measure doxorubicin levels, tumors were homogenized and doxorubicin was extracted using acidified methanol (1% acetic acid). Samples were vortexed and then placed at −80 °C for 1 hour. Samples were then centrifuged for 10 minutes and the supernatant was analyzed by HPLC.

Biodistribution and Pharmacokinetics Studies

Twenty mg/kg MU-P equivalents in a volume of 0.2 mL were injected via tail vein into CD-1 mice. For pharmacokinetic studies, blood was collected 10, 20, 60, 180, 1440 and 2880 minutes (3 mice per group) after injection and centrifuged for 10 min at 15,000 g. Serum was collected in a tube with a 1:100 dilution of Phosphatase Inhibitor Cocktail 2 (Sigma). Ten μL of serum was added to 2 mL of HBS along with 10 μL of a 15% $C_{12}E_{10}$

solution. A standard curve was made by titrating MU-P loaded liposomes into the serum from an untreated mouse. MU-P were measured from each serum sample. The data was fit to a two-compartment model using GraphPad Prism. For biodistribution studies, tissues were isolated and flash frozen 3 and 48 hours after injection.

Supplementary Material

Refer to Web version on PubMed Central for supplementary material.

Acknowledgments

References

1. Allen TM, Cullis PR. Liposomal drug delivery systems: from concept to clinical applications. Adv Drug Deliv Rev. 2013; 65:36–48. [PubMed: 23036225]

2. Ernsting MJ, Murakami M, Roy A, Li SD. Factors controlling the pharmacokinetics, biodistribution and intratumoral penetration of nanoparticles. J Control Release. 2013; 172:782–794. [PubMed: 24075927]

3. Jain RK, Stylianopoulos T. Delivering nanomedicine to solid tumors. Nat Rev Clin Oncol. 2010; 7:653–664. [PubMed: 20838415]

4. Minchinton AI, Tannock IF. Drug penetration in solid tumours. Nat Rev Cancer. 2006; 6:583–592. [PubMed: 16862189]

5. Heldin CH, Rubin K, Pietras K, Ostman A. High interstitial fluid pressure - an obstacle in cancer therapy. Nat Rev Cancer. 2004; 4:806–813. [PubMed: 15510161]

6. Sugahara KN, Teesalu T, Karmali PP, Kotamraju VR, Agemy L, Greenwald DR, et al. Coadministration of a tumor-penetrating peptide enhances the efficacy of cancer drugs. Science. 2010; 328:1031–1035. [PubMed: 20378772]

7. Paoli EE, Ingham ES, Zhang H, Mahakian LM, Fite BZ, Gagnon MK, et al. Accumulation, internalization and therapeutic efficacy of neuropilin-1-targeted liposomes. J Control Release. 2014; 178:108–117. [PubMed: 24434424]

8. Gao H, Yang Z, Zhang S, Cao S, Pang Z, Yang X, et al. Glioma-homing peptide with a cell-penetrating effect for targeting delivery with enhanced glioma localization, penetration and suppression of glioma growth. J Control Release. 2013; 172:921–928. [PubMed: 24120853]

9. Wang S, Shin IS, Hancock H, Jang BS, Kim HS, Lee SM, et al. Pulsed high intensity focused ultrasound increases penetration and therapeutic efficacy of monoclonal antibodies in murine xenograft tumors. J Control Release. 2012; 162:218–224. [PubMed: 22732476]

10. Li L, ten Hagen TLM, Bolkestein M, Gasselhuber A, Yatvin J, van Rhoon GC, et al. Improved intratumoral nanoparticle extravasation and penetration by mild hyperthermia. J Control Release. 2013; 167:130–137. [PubMed: 23391444]

11. Wong C, Stylianopoulos T, Cui J, Martin J, Chauhan VP, Jiang W, et al. Multistage nanoparticle delivery system for deep penetration into tumor tissue. Proc Natl Acad Sci USA. 2011; 108:2426–2431. [PubMed: 21245339]

12. Mok W, Boucher Y, Jain RK. Matrix metalloproteinases-1 and -8 improve the distribution and efficacy of an oncolytic virus. Cancer Res. 2007; 67:10664–10668. [PubMed: 18006807]

13. Olive KP, Jacobetz MA, Davidson CJ, Gopinathan A, McIntyre D, Honess D, et al. Inhibition of Hedgehog signaling enhances delivery of chemotherapy in a mouse model of pancreatic cancer. Science. 2009; 324:1457–1461. [PubMed: 19460966]

14. Diop-Frimpong B, Chauhan VP, Krane S, Boucher Y, Jain RK. Losartan inhibits collagen I synthesis and improves the distribution and efficacy of nanotherapeutics in tumors. Proc Natl Acad Sci USA. 2011; 108:2909–2914. [PubMed: 21282607]

15. McKee TD, Grandi P, Mok W, Alexandrakis G, Insin N, Zimmer JP, et al. Degradation of fibrillar collagen in a human melanoma xenograft improves the efficacy of an oncolytic herpes simplex virus vector. Cancer Res. 2006; 66:2509–2513. [PubMed: 16510565]

16. Liu J, Liao S, Diop-Frimpong B, Chen W, Goel S, Naxerova K, et al. TGF-β blockade improves the distribution and efficacy of therapeutics in breast carcinoma by normalizing the tumor stroma. Proc Natl Acad Sci USA. 2012; 109:16618–16623. [PubMed: 22996328]

17. Roy Chaudhuri T, Arnold RD, Yang J, Turowski SG, Qu Y, Spernyak JA, et al. Mechanisms of tumor vascular priming by a nanoparticulate doxorubicin formulation. Pharm Res. 2012; 29:3312–3324. [PubMed: 22798260]

18. Pastuskovas CV, Mundo EE, Williams SP, Nayak TK, Ho J, Ulufatu S, et al. Effects of anti-VEGF on pharmacokinetics, biodistribution and tumor penetration of trastuzumab in a preclinical breast cancer model. Mol Cancer Ther. 2012; 11:752–762. [PubMed: 22222630]

19. Chauhan VP, Stylianopoulos T, Martin JD, Popovic Z, Chen O, Kamoun WS, et al. Normalization of tumour blood vessels improves the delivery of nanomedicines in a size-dependent manner. Nat Nanotechnol. 2012; 7:383–388. [PubMed: 22484912]

20. Maeda H, Bharate GY, Daruwalla J. Polymeric drugs for efficient tumor-targeted drug delivery based on EPR-effect. European Journal of Pharmaceutics and Biopharmaceutics. 2009; 71:409–419. [PubMed: 19070661]

21. Yuan F, Leunig M, Huang SK, Berk DA, Papahadjopoulos D, Jain RK. Microvascular permeability and interstitial penetration of sterically stabilized (stealth) liposomes in a human tumor xenograft. Cancer Res. 1994; 54:3352–3356. [PubMed: 8012948]

22. Pirinen RT, Tammi RH, Tammi MI, Pääkkö PK, Parkkinen JJ, Agren UM, et al. Expression of hyaluronan in normal and dysplastic bronchial epithelium and in squamous cell carcinoma of the lung. Int J Cancer. 1998; 79:251–255. [PubMed: 9645346]

23. Ropponen K, Tammi M, Parkkinen J, Eskelinen M, Tammi R, Lipponen P, et al. Tumor cell-associated hyaluronan as an unfavorable prognostic factor in colorectal cancer. Cancer Res. 1998; 58:342–347. [PubMed: 9443415]

24. Setälä LP, Tammi MI, Tammi RH, Eskelinen MJ, Lipponen PK, Agren UM, et al. Hyaluronan expression in gastric cancer cells is associated with local and nodal spread and reduced survival rate. Br J Cancer. 1999; 79:1133–1138. [PubMed: 10098747]

25. Anttila MA, Tammi RH, Tammi MI, Syrjänen KJ, Saarikoski SV, Kosma VM. High levels of stromal hyaluronan predict poor disease outcome in epithelial ovarian cancer. Cancer Res. 2000; 60:150–155. [PubMed: 10646867]

26. Auvinen P, Tammi R, Parkkinen J, Tammi M, Agren U, Johansson R, et al. Hyaluronan in peritumoral stroma and malignant cells associates with breast cancer spreading and predicts survival. Am J Pathol. 2000; 156:529–536. [PubMed: 10666382]

27. Mahadevan D, Von Hoff DD. Tumor-stroma interactions in pancreatic ductal adenocarcinoma. Mol Cancer Ther. 2007; 6:1186–1197. [PubMed: 17406031]

28. Shepard MH, Frost GI, Rybak ME, Ramanathan RK, Von Hoff DD, Infante J, et al. Targeting hyaluronan (HA) in the tumor stroma. Translational evaluation of pegylated hyaluronidase (PEGPH20) in animal models and patients with advanced solid tumors. EORTC Florida. 2010:1–1.

29. Mummert ME, Mummert DI, Ellinger L, Takashima A. Functional Roles of Hyaluronan in B16-F10 Melanoma Growth and Experimental Metastasis in Mice. Mol Cancer Ther. 2003; 2:295–300. [PubMed: 12657724]

30. Arai E, Nishida Y, Wasa J, Urakawa H, Zhuo L, Kimata K, et al. Inhibition of hyaluronan retention by 4-methylumbelliferone suppresses osteosarcoma cells in vitro and lung metastasis in vivo. Br J Cancer. 2011; 105:1839–1849. [PubMed: 22045192]

31. Pályi-Krekk Z, Barok M, Isola J, Tammi M, Szöllosi J, Nagy P. Hyaluronan-induced masking of ErbB2 and CD44-enhanced trastuzumab internalisation in trastuzumab resistant breast cancer. Eur J Cancer. 2007; 43:2423–2433. [PubMed: 17911008]

32. Thompson CB, Shepard HM, O'Connor PM, Kadhim S, Jiang P, Osgood RJ, et al. Enzymatic depletion of tumor hyaluronan induces antitumor responses in preclinical animal models. Mol Cancer Ther. 2010; 9:3052–3064. [PubMed: 20978165]

33. Lokeshwar VB, Lopez LE, Munoz D, Chi A, Shirodkar SP, Lokeshwar SD, et al. Antitumor activity of hyaluronic acid synthesis inhibitor 4-methylumbelliferone in prostate cancer cells. Cancer Res. 2010; 70:2613–2623. [PubMed: 20332231]

34. Beckenlehner K, Bannke S, Spruss T, Bernhardt G, Schönenberg H, Schiess W. Hyaluronidase enhances the activity of adriamycin in breast cancer models in vitro and in vivo. J Cancer Res Clin Oncol. 1992; 118:591–596. [PubMed: 1517281]

35. Provenzano PP, Cuevas C, Chang AE, Goel VK, Von Hoff DD, Hingorani SR. Enzymatic targeting of the stroma ablates physical barriers to treatment of pancreatic ductal adenocarcinoma. Cancer Cell. 2012; 21:418–429. [PubMed: 22439937]

36. Eikenes L, Bruland ØS, Brekken C, de C, Davies L. Collagenase increases the transcapillary pressure gradient and improves the uptake and distribution of monoclonal antibodies in human osteosarcoma xenografts. Cancer Res. 2004; 64:4768–4773. [PubMed: 15256445]

37. Hiraga T, Ito S, Nakamura H. Cancer stem-like cell marker CD44 promotes bone metastases by enhancing tumorigenicity, cell motility, and hyaluronan production. Cancer Res. 2013; 73:4112–4122. [PubMed: 23633482]

38. Okuda H, Kobayashi A, Xia B, Watabe M, Pai SK, Hirota S, et al. Hyaluronan synthase HAS2 promotes tumor progression in bone by stimulating the interaction of breast cancer stem-like cells with macrophages and stromal cells. Cancer Res. 2012; 72:537–547. [PubMed: 22113945]

39. Twarock S, Freudenberger T, Poscher E, Dai G, Jannasch K, Dullin C, et al. Inhibition of oesophageal squamous cell carcinoma progression by in vivo targeting of hyaluronan synthesis. Mol Cancer. 2011; 10:30. [PubMed: 21429221]

40. Yoshihara S, Kon A, Kudo D, Nakazawa H, Kakizaki I, Sasaki M, et al. A hyaluronan synthase suppressor, 4-methylumbelliferone, inhibits liver metastasis of melanoma cells. FEBS Lett. 2005; 579:2722–2726. [PubMed: 15862315]

41. Kudo D, Kon A, Yoshihara S, Kakizaki I, Sasaki M, Endo M, et al. Effect of a hyaluronan synthase suppressor, 4-methylumbelliferone, on B16F-10 melanoma cell adhesion and locomotion. Biochem Biophys Res Commun. 2004; 321:783–787. [PubMed: 15358095]

42. Nakazawa H, Yoshihara S, Kudo D, Morohashi H, Kakizaki I, Kon A, et al. 4-methylumbelliferone, a hyaluronan synthase suppressor, enhances the anticancer activity of gemcitabine in human pancreatic cancer cells. Cancer Chemother Pharmacol. 2006; 57:165–170. [PubMed: 16341905]

43. Morohashi H, Kon A, Nakai M, Yamaguchi M, Kakizaki I, Yoshihara S, et al. Study of hyaluronan synthase inhibitor, 4-methylumbelliferone derivatives on human pancreatic cancer cell (KP1-NL). Biochem Biophys Res Commun. 2006; 345:1454–1459. [PubMed: 16730656]

44. Zamek-Gliszczynski MJ, Nezasa KI, Tian X, Kalvass JC, Patel NJ, Raub TJ, et al. The important role of Bcrp (Abcg2) in the biliary excretion of sulfate and glucuronide metabolites of acetaminophen, 4-methylumbelliferone, and harmol in mice. Mol Pharmacol. 2006; 70:2127–2133. [PubMed: 16959944]

45. Uchaipichat V, Mackenzie PI, Guo XH, Gardner-Stephen D, Galetin A, Houston JB, et al. Human udp-glucuronosyltransferases: isoform selectivity and kinetics of 4-methylumbelliferone and 1-naphthol glucuronidation, effects of organic solvents, and inhibition by diclofenac and probenecid. Drug Metab Dispos. 2004; 32:413–423. [PubMed: 15039294]

46. Abate A, Dimartino V, Spina P, Costa PL, Lombardo C, Santini A, et al. Hymecromone in the treatment of motor disorders of the bile ducts: a multicenter, double-blind, placebo-controlled clinical study. Drugs Exp Clin Res. 2001; 27:223–231. [PubMed: 11951580]

47. Garrett ER, Venitz J, Eberst K, Cerda JJ. Pharmacokinetics and bioavailabilities of hymecromone in human volunteers. Biopharm Drug Dispos. 1993; 14:13–39. [PubMed: 8427942]

48. Kostova IP, Manolov II, Nicolova IN, Danchev ND. New metal complexes of 4-methyl-7-hydroxycoumarin sodium salt and their pharmacological activity. Farmaco. 2001; 56:707–713. [PubMed: 11680816]

49. Kultti A, Pasonen-Seppänen S, Jauhiainen M, Rilla KJ, Kärnä R, Pyöriä E, et al. 4-Methylumbelliferone inhibits hyaluronan synthesis by depletion of cellular UDP-glucuronic acid and downregulation of hyaluronan synthase 2 and 3. Exp Cell Res. 2009; 315:1914–1923. [PubMed: 19285976]

50. Crielaard BJ, van der Wal S, Le HT, Bode ATL, Lammers T, Hennink WE, et al. Liposomes as carriers for colchicine-derived prodrugs: vascular disrupting nanomedicines with tailorable drug release kinetics. Eur J Pharm Sci. 2012; 45:429–435. [PubMed: 21907797]

51. Kohli AG, Kieler-Ferguson HM, Chan D, Szoka FC. A robust and quantitative method for tracking liposome contents after intravenous administration. J Control Release. 2014; 176:86–93. [PubMed: 24368300]

52. Tao K, Fang M, Alroy J, Sahagian GG. Imagable 4T1 model for the study of late stage breast cancer. BMC Cancer. 2008; 8:228. [PubMed: 18691423]

53. Naba A, Clauser KR, Hoersch S, Liu H, Carr SA, Hynes RO. The matrisome: in silico definition and in vivo characterization by proteomics of normal and tumor extracellular matrices. Mol Cell Proteomics. 2012; 11:M111.014647. [PubMed: 22159717]

54. Baish JW, Stylianopoulos T, Lanning RM, Kamoun WS, Fukumura D, Munn LL, et al. Scaling rules for diffusive drug delivery in tumor and normal tissues. Proc Natl Acad Sci USA. 2011; 108:1799–1803. [PubMed: 21224417]

55. Provenzano PP, Hingorani SR. Hyaluronan, fluid pressure, and stromal resistance in pancreas cancer. Br J Cancer. 2013; 108:1–8. [PubMed: 23299539]

56. Eikenes L, Tari M, Tufto I, Bruland ØS, de Lange Davies C. Hyaluronidase induces a transcapillary pressure gradient and improves the distribution and uptake of liposomal doxorubicin (Caelyx) in human osteosarcoma xenografts. Br J Cancer. 2005; 93:81–88. [PubMed: 15942637]

57. Jiang D, Liang J, Noble PW. Hyaluronan in tissue injury and repair. Annu Rev Cell Dev Biol. 2007; 23:435–461. [PubMed: 17506690]

58. Jadin L, Bookbinder LH, Frost GI. A comprehensive model of hyaluronan turnover in the mouse. Matrix Biol. 2012; 31:81–89. [PubMed: 22142621]

59. Lin W, Shuster S, Maibach HI, Stern R. Patterns of hyaluronan staining are modified by fixation techniques. J Histochem Cytochem. 1997; 45:1157–1163. [PubMed: 9267476]

60. Schindelin J, Arganda-Carreras I, Frise E, Kaynig V, Longair M, Pietzsch T, et al. Fiji: an open-source platform for biological-image analysis. Nat Meth. 2012; 9:676–682.

61. Manders E, Verbeek FJ, Aten JA. Measurement of co- localization of objects in dual- colour confocal images. Journal of Microscopy. 1993; 169:375–382.

62. Feldman JP, Goldwasser R, Mark S, Schwartz J, Orion I. A mathematical model for tumor volume evaluation using two-dimensions. J Appl Quant Methods. 2009; 4:455–462.
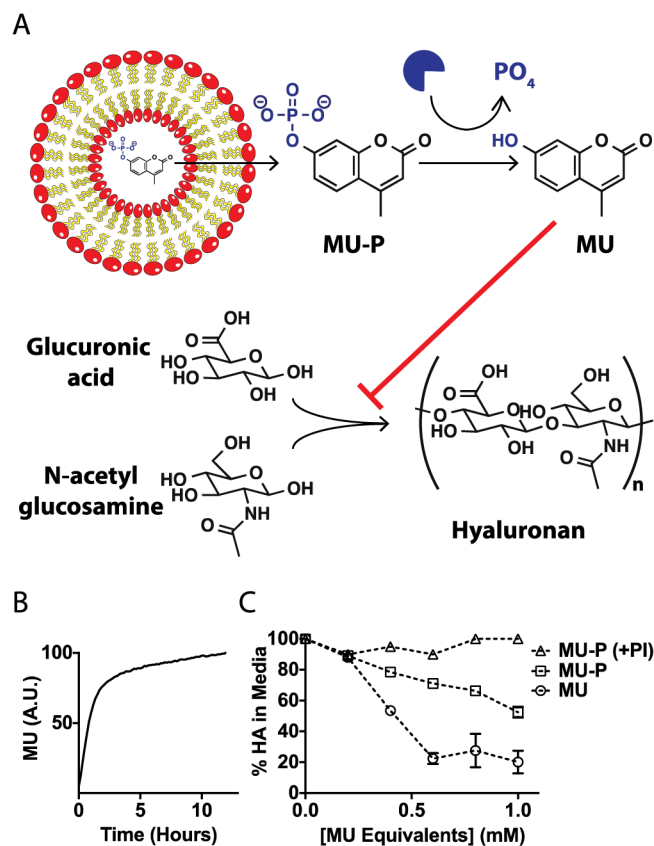
Figure 1. MU-P is rapidly converted to MU by phosphatases and inhibits HA synthesis
(A) MU-P is encapsulated in liposomes and rapidly converted to MU upon release; MU inhibits HA synthesis. (B) MU-P is rapidly converted to MU in serum and (C) both MU and MU-P deplete HA in culture media (n=3). Addition of a phosphatase inhibitor (PI) abolishes the activity of MU-P.
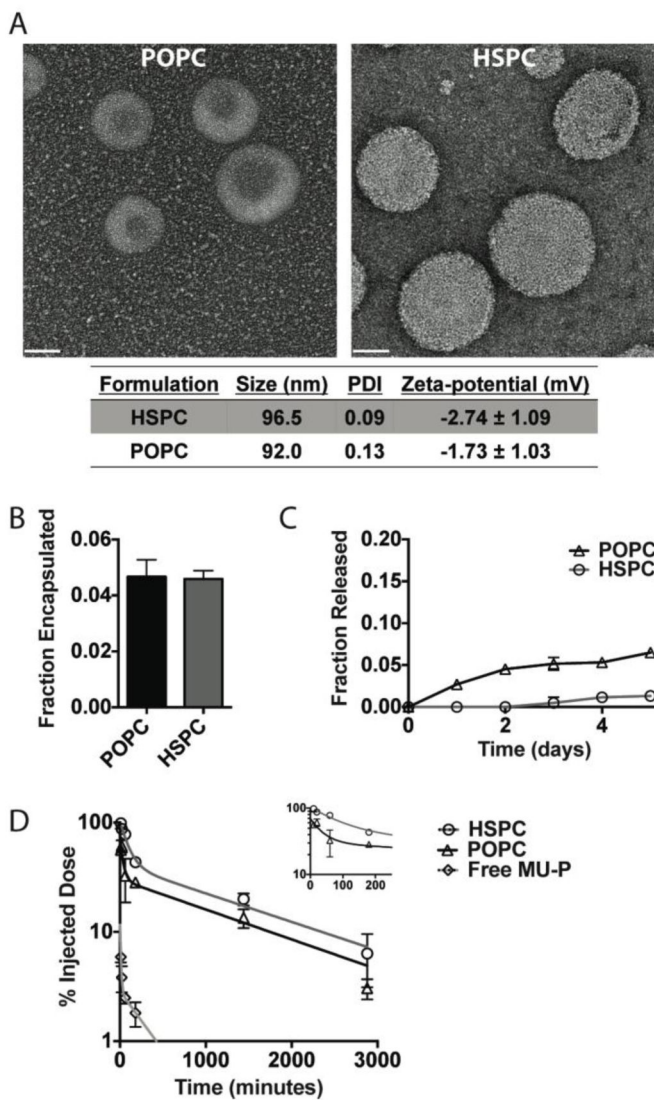
Figure 2. Characterization of MU-P liposomes
(A) TEM images of POPC:Cholesterol and HSPC:Cholesterol liposomes encapsulating MU-P (top) and summary of liposome characteristics including polydispersity index (PDI), diameter, and surface potential (table, n=3). Scale bar is 50 μm. (B) MU-P is passively encapsulated in both liposomes to a similar extent (n=3), but (C) leaks more quickly from POPC liposomes in the presence of serum at 37°C. (D) Both HSPC and POPC MU-P liposomes have extended circulation times compared to free MU-P. Inset shows early timepoints of HSPC and POPC liposome leakage.
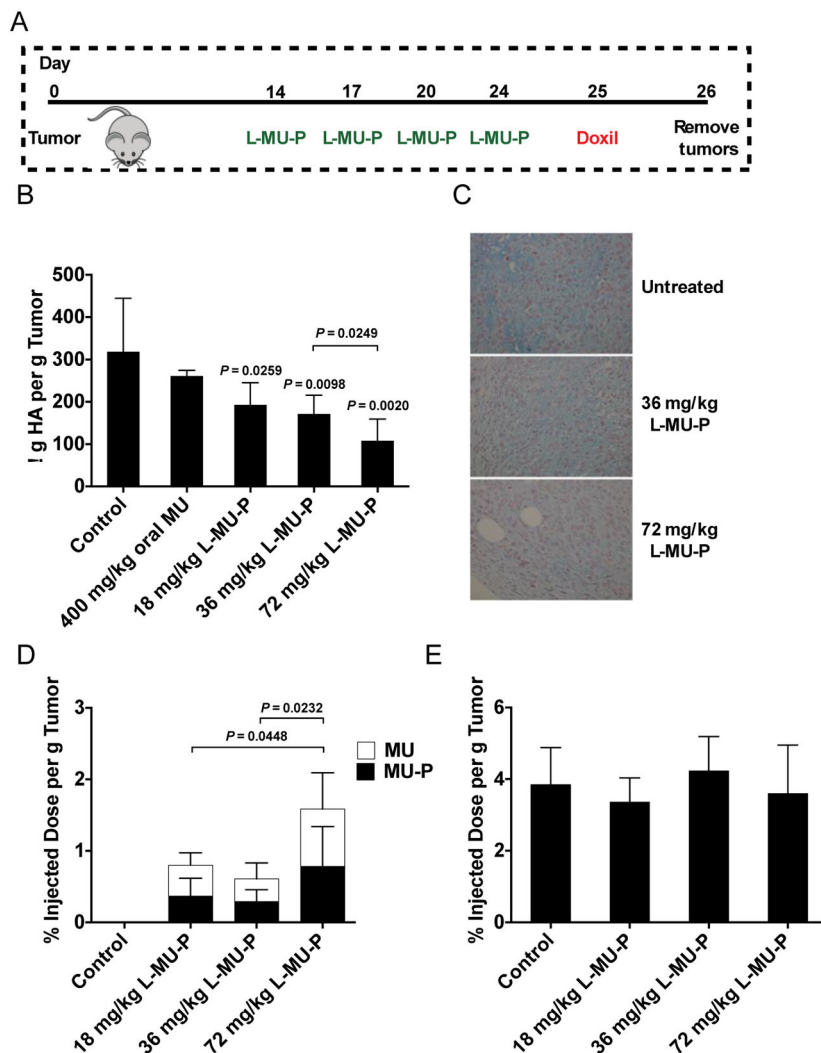
Figure 3. L-MU-P depletes HA in 4T1 tumors
(A) Mice with orthotopic 4T1 tumors were given 1–4 doses of L-MU-P according to the given schedule or oral MU daily. A single dose of doxorubicin was administered to measure liposome uptake into tumors (n=10). (B) L-MU-P significantly reduced HA levels in 4T1 tumors as compared to oral gavage of MU. This reduction occurred in a dose dependent manner as measured by an HA-specific ELISA assay or (C) Alcian Blue staining. (D) MU-P and MU accumulate in the tumor in a dose dependent manner, while (E) Doxil® accumulation is not affected by HA levels. Statistical analyses were performed with (D) Student's t test (B) or ANOVA and are relative to oral MU. Error bars denote mean ± standard deviation.
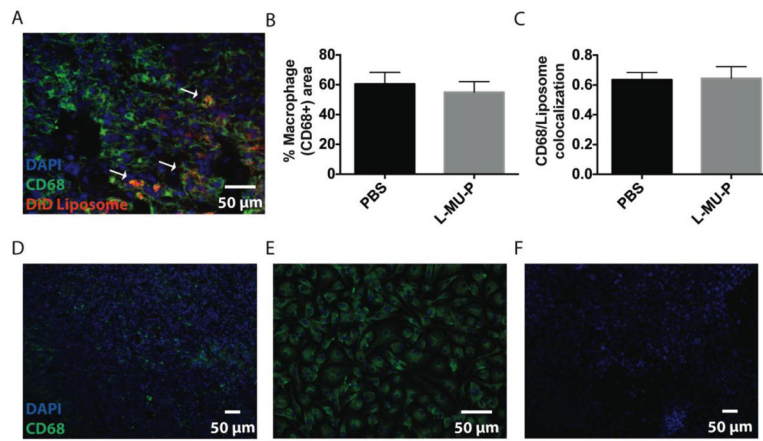
Figure 4. Liposome localization in endogenous 4T1 tumor macrophages
(A) Liposomes colocalize with 4T1 tumor macrophages. White arrows highlight areas of colocalization. (B) HA depletion with L-MU-P does not alter tumor macrophage content or (C) liposome colocalization with tumor macrophages. (D) 4T1 tumor sections show macrophage staining. (E) Primary bone marrow macrophages in culture are positive for CD68 while (F) 4T1 tumor cells are not.
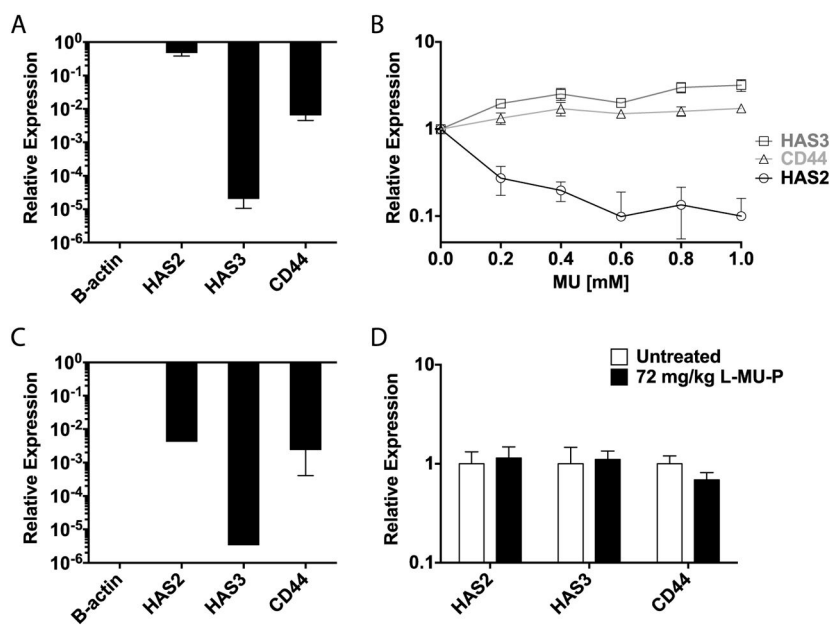
Figure 5. L-MU-P modulates gene expression *in vitro*, but not *in vivo*.
Gene expression levels were examined by qRT-PCR. (A) *HAS2* is the most abundant HA-synthase in cell culture. (B) MU down regulates expression of *HAS2 in vitro* (n=3). (C) *HAS2* is the most abundant HA-synthase in 4T1 orthotopic tumors, but (D) L-MU-P has no effect on its expression *in vivo* (n=10).
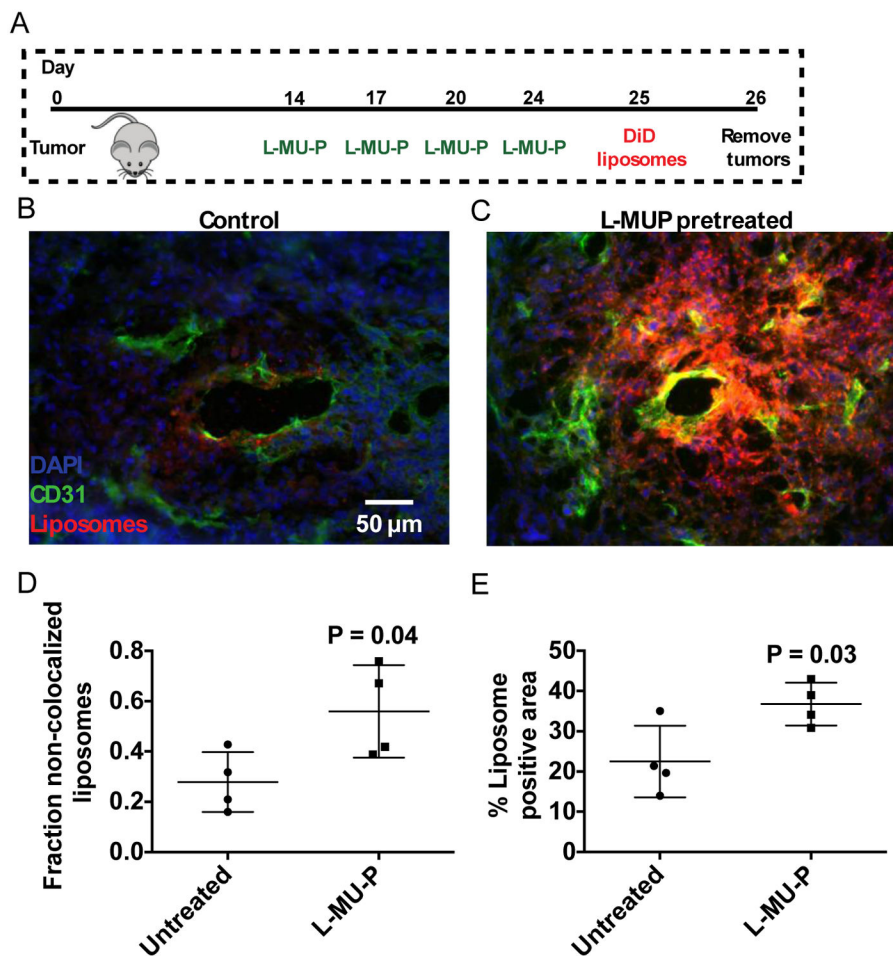
Figure 6. HA depletion improves liposome distribution in 4T1 tumors
(A) Orthotopic 4T1 tumors were treated with 4 doses of L-MU-P followed by a single dose of fluorescently labeled liposomes (n=4). (B) Liposome penetration in control tumors is less pronounced than in (C) tumors with reduced HA. (D) Liposome distribution quantified by colocalization analysis across the entire tumor as well as by (E) percent area analysis across the entire tumor. Statistical analyses were performed with Student's t-test. Error bars denote mean ± standard deviation.
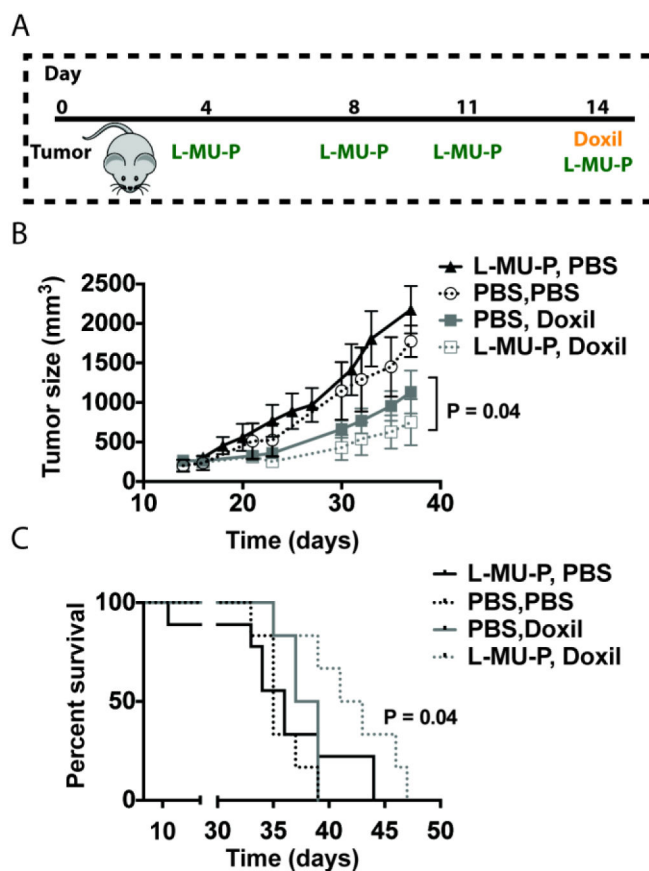
Figure 7. Improved liposome distribution following HA depletion improves efficacy of Doxil®
(A) 4T1 orthotopic tumors were treated with 4 doses of L-MU-P followed by a single dose of Doxil® at 6 mg/kg (n=6). (B) When combined with Doxil®, HA depletion by L-MU-P statistically reduced primary tumor growth and (C) extended overall survival. Statistical analyses were performed with (B) Student's t-test (C) or Log-rank (Mantel-Cox) test. Error bars denote mean ± standard deviation.